Hindawi
Mathematical Problems in Engineering
Volume 2022, Article ID 6392909, 14 pages
https://doi.org/10.1155/2022/6392909

Research Article

Comparative Study on Triaxial Test of Undisturbed and Remolded Loess

Shuo Zhang,[1] Chunhang Liang,[2] Chao Zheng,[1] and Juyun Zhai[1]

[1]*School of Civil and Transportation Engineering, Henan University of Urban Construction, Pingdingshan 467002, China*
[2]*School of Civil Engineering and Architecture, Henan University, Kaifeng 475000, China*

Correspondence should be addressed to Chunhang Liang; chliang@henu.edu.cn

Received 11 January 2022; Revised 12 February 2022; Accepted 18 February 2022; Published 11 April 2022

Academic Editor: Gengxin Sun

The difference of sample preparation methods will directly lead to the difference of the structure of the sample, and the mechanical response characteristics under external load will be different. Based on the conventional tests such as particle analysis, specific gravity, critical moisture content, and consolidation test of undisturbed loess from Xi'an, this paper focuses on the static triaxial consolidated drained shear and consolidated undrained shear tests on undisturbed and remolded loess. The results show that: (1) the structure has an obvious influence on the stress-strain relationship of the sample, the stress-strain curve of the undisturbed sample is a strain softening curve, and the stress-strain curve of the remolded sample is a weak strain hardening curve; (2) under the same loading conditions, the triaxial shear strength of the undisturbed soil is significantly higher than that of the remolded soil; (3) the change rule of the consolidation ratio of undisturbed and remolded samples is basically the same, but the final consolidation ratio of remolded soil is greater than that of undisturbed soil.

1. Introduction

The measurement methods of mechanical characteristic parameters of soil are divided into in-situ test and laboratory test [1, 2]. In the in-situ test, the stress state of soil is close to its real stress state. However, its boundary conditions cannot be accurately controlled and cannot reflect the stress-strain relationship of soil in other stress-strain states. But by comparison, the boundary conditions of indoor test are relatively clear and easy to control, and the research results of soil indoor test are quite rich [3–7]. Remarkably, the preparation method of soil sample is an important factor affecting the determination results of soil laboratory test. Soil samples are divided into undisturbed soil samples and remolded soil samples. The original structure of cohesive soil can be well maintained during sampling and sample preparation, so undisturbed soil samples are used comprehensively. For soil samples with less cohesion, the original shape of undisturbed samples cannot be maintained during sampling and sample preparation. Therefore, remolded soil samples are mostly used in laboratory tests.

Natural soil forms structural deformation due to the influence of soil deposition history and surrounding environmental changes. Mitchell et al. defined the structure of a soil mass as "tectonic" and "joint," which shows the arrangement of soil particles and interactions between soil particles [8]. Burland insisted that, like the initial void ratio and stress history, the structure had a significant impact on the mechanical properties of undisturbed soil [9]. Ovalle and Arenaldi-Perisic introduced the behavior of natural diatomite under compression, shear and cyclic loads, and the new opinion of undisturbed high plastic diatomite sludge in Mejillones Bay, Northern Chile [10]. Sousa et al. gave the column test results on large undisturbed samples [11]. Freitas et al. introduced the coefficient of pore expansion to correct the possible differences in measuring the total pore volume under dry or water-saturated conditions [12]. Xu et al. proposed a new method for measuring the preconsolidation pressure of structural loess soil [13]. Aiming at the collapse potential of Gorgan loess, Haeri et al. studied the undisturbed and remolded samples by using the consolidation instrument test [14]. Gao et al. investigated the strength and deformation characteristics of undisturbed unsaturated loess under

different moisture content conditions [15]. Chu studied the engineering characteristics of coarse-grained soil, such as strength and deformation [16]. Airey conducted conventional and stress path triaxial tests on cemented carbonate soil obtained from the northwest shelf of Australia and found that the dry density and cementation degree of natural calcareous rock samples vary greatly [17]. Chen et al. systematically studied the mesostructure evolution characteristics of expansive soil and loess under different stress paths, dry wet cycle, immersion expansion, and inundation collapse conditions by using CT triaxial apparatus [18]. Nokande et al. tested different types of soil [19]. Wang et al. studied the different dry densities of undisturbed soil and remolded soil through oedometer test, hydraulic conductivity test, and field emission scanning electron microscope [20]. Jiang et al. studied the effect of structure on secondary compressibility during pressure change [21].

Based on the conventional tests such as particle analysis, specific gravity, limit moisture content, and consolidation test of undisturbed loess from Xi'an, we focus on the static triaxial consolidated drained shear and consolidated undrained shear tests of undisturbed and remolded loess. And in order to explore the influence of structure on the results of indoor triaxial test, we analyze the differences between them in the test results of stress-strain relationship, stress path, shear strength index, and consolidation ratio.

2. Specimen Preparation and Test Plan

2.1. The Location of Sample Collection. Sampling work is carried out at the tunnel face 1 m from the tunnel top and 2 open excavation foundation pits. The sampling depths are 12 m and 13 m, respectively, and both of them are loess soil (2-1-2) samples. The sample collection is shown in Table 1. We collect about 30 kg remolded samples and 6 undisturbed samples, including 3 tunnel faces and 3 open excavation foundation pits. All the samples are sealed with plastic film after on-site collection.

According to the requirements of test contents in Table 2, the axial principal stress of triaxial compression test sample is set by the sampling depth. Therefore, the total overburden stress at the sampling point is calculated based on the field sampling depth, overburden type, thickness, and density. The specific calculation results are shown in Table 2.

2.2. Determination of Test Scheme. Considering the test content requirements in Table 3, firstly the triaxial compression test sample shall be subject to K_0 consolidation, and the K_0 shall be determined based on the survey report. Secondly, the consolidation test results shall be sorted out with basic physical property parameters. The test scheme is shown in Table 3.

3. Basic Physical Property Test

3.1. Water Content Test. According to the standard for geotechnical test methods (GB/T 50123-2019), the moisture content of this test adopts the drying method, and the temperature is 105°C, and the weighing accuracy is 0.01 g. The test results are shown in Table 4. The parallel difference of water content of sample D14-01 is 0.26%, less than 1.0%, which meets the specification requirements. The parallel difference of moisture content of sample D14-02 is 0.38%, less than 1.0%, which meets the specification requirements.

3.2. Density Test. According to the standard for geotechnical test methods (GB/T 50123-2019), the ring knife method is adopted in this test, and the weighing accuracy is 0.01 g. The test results are shown in Table 5. The density parallel difference of sample D14-01 is 0.01 g/cm^3, and the density parallel difference of sample D14-02 is 0.01 g/cm^3, less than 0.03 g/cm^3, which all meet the specification requirements.

3.3. Limit Moisture Content Test. According to the standard for geotechnical test methods (GB/T 50123-2019), the liquid plastic limit combined tester method is adopted in the limit moisture content of this test, and the moisture content adopts the drying method. In addition, the drying temperature is 105°C, and the weighing accuracy is 0.01 g. The test results are shown in Table 6.

3.4. Particle Analysis Tests. The better size 2,600 laser particle size analyzer (wet method) is used for particle size analysis in this experiment. The analysis results are shown in Figure 1. The particle compositions and contents of sample D14-01 and sample D14-02 are shown in Table 7.

3.5. Consolidation Test. According to the standard for geotechnical test methods (GB/T 50123-2019), the standard consolidation test is adopted for the consolidation test of undisturbed samples, and the deformation measurement accuracy is 0.01 mm. The specific test scheme is shown in Table 8.

The undisturbed specimen has a diameter of 61.8 mm and a height of 20 mm. The test instrument is WG (GDG-4S) horizontal bar consolidation instrument (triple high pressure). The stability standard is based on 24 hours of consolidation under each level of pressure or the hourly change of sample deformation shall not be greater than 0.01 mm. Figures 2 and 3 are e-lgp curves of CT-01 and CT-02 consolidation tests of undisturbed samples, respectively. It is calculated that the compression modulus $E_{s1\text{-}2}$ of undisturbed sample CT-01 of sample D14-01 is 8.91 MPa and the compression coefficient $a_{1\text{-}2}$ is 0.2 MPa^{-1}. It belongs to medium compressible soil. The early consolidation pressure PC is 288.4 kPa determined by the CASA grant graphical method. The compression modulus $E_{s1\text{-}2}$ of undisturbed sample CT-02 of sample D14-02 is 9.18 MPa and the compression coefficient is 0.18 MPa^{-1}. It belongs to medium compressible soil, and its preconsolidation pressure PC is 302.0 kPa determined by the CASA grant graphical method.

4. Three-Axis Compression Nondrainage Test

4.1. Pilot Protocol. According to the test requirements, the triaxial compression tests of undisturbed and remolded samples are carried out. The specific test scheme is shown in Table 9.

Table 1: Sample collection.

Sample no.	Sample location	Sample elevation (m)	Sample depth (m)	Sample type	Sample soil layers and layer numbers
D14-01	Tunnel face, 1 m from tunnel top	371.00	12	Undisturbed sample, remolded sample	Loess-like soil (2-1-2)
D14-02	Open cut foundation pit	367.00	13	Undisturbed sample, remolded sample	Loess-like soil (2-1-2)

Table 2: Calculation of total stress on specimen.

Sample no.	Total stress overlying			
	Distribution of overlying rock and soil layers	Thickness (m)	Density (g/cm^3)	Total stress overlying (kPa)
D14-01	Miscellaneous soil filling	1.9	1.80	204
	Loess-like soil (2-1-1)	3.8	35	
	Loess-like soil (2-1-2)	6.3	1.76	
D14-02	Miscellaneous soil filling	1.9	1.80	221
	Loess-like soil (2-1-1)	3.8	35	
	Loess-like soil (2-1-2)	7.3	1.76	

Table 3: General test scheme table.

Test no.	Test name	Test content
1	Testing of the basic physical properties of soil	Moisture content, density, limit moisture content, particle analysis, and consolidation test
2	Three-axis compression test (TC)	Stress-strain relationship, consolidation ratio, and stress path

Table 4: Water content test record.

Sample no.	Box no.	Box quality (g)	Box humidified soil quality (g)	Box plus dry soil mass (g)	Moisture quality (g)	Dry soil quality m_d (g)	Moisture content ω (%)	Average moisture content $\overline{\omega}$ (%)
D14-01	A06	13.50	33.84	30.47	3.37	16.97	19.86	19.73
	A15	13.11	29.22	26.58	2.64	13.47	19.6	
D14-02	A09	13.24	24.82	22.79	2.03	9.55	21.26	21.07
	A17	13.34	25.38	23.3	2.08	9.96	20.88	

Table 5: Density test record (ring knife method).

Sample no.	Ring knife volume (cm^3)	Ring knife quality (g)	Ring knife humidifies soil quality (g)	Wet soil quality (g)	Wet density ρ (g/cm^3)	Water content ω (%)	Dry density ρ_d (g/cm^3)	Average dry density $\overline{\rho_d}$ (g/cm^3)
D14-01	60	44.62	150.16	105.4	1.76	19.73	37	37
	60	43.08	148.86	105.78	1.75	19.73	36	
D14-02	60	43.95	159.04	115.09	1.92	21.07	39	39
	60	44.62	160.35	115.73	1.93	21.07	39	

Table 6: Density test record (ring knife method).

Sample no.	Depth of cone sinking h (mm)	Box no.	Wet soil quality m_0 (g)	Drying soil quality m_d (g)	Water content ω (%)	Liquid limits ω_L (%)	Plastic limit ω_P (%)	Plasticity index I_P
D14-01	3.6	A02	10.30	8.45	21.89	30.4	17.0	13.4
	8.1	A17	14.34	11.25	27.47			
	13.0	A15	137	8.68	33.29			
D14-02	4.3	A19	14.52	11.83	22.75	32	16.2	15.1
	8.6	A16	8.87	6.90	28.55			
	13.3	A12	14.33	10.64	34.61			

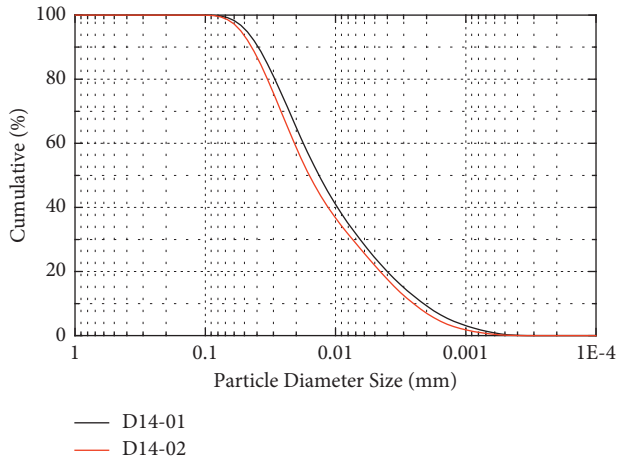

Figure 1: Particle analysis curve.

Table 7: Fractions and contents.

No.	Granules and content (%)		
	Sand	Powder grains	Sticky particles
D14-01	0.34	75.31	24.35
D14-02	0.61	77.48	21.91

Table 8: Consolidation test scheme.

Sample no.	Sample no.	Test no.	Pressurized rating (kPa)
D14-01	Undisturbed	CT-01	12.5, 25, 50, 100, 200, 400, 800, 1,600, 3,200
D14-02	Undisturbed	T-02	

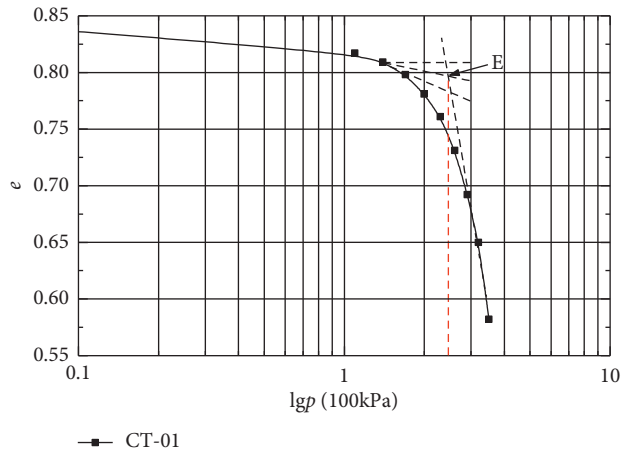

Figure 2: e-lgp curve of CT-01 of intact sample.

4.2. Specimen Preparation and Test Instruments. The diameter of undisturbed and remolded specimens is 39.1 mm and the height is 80 mm. The remolded sample shall be prepared by controlling the dry density (dry density of undisturbed sample), and the prepared sample shall be placed in the petri dish for more than 48 hours.

The test instrument is a SLB-1A stress-strain controlled triaxial creep instrument. As shown in Figure 4, the test instrument consists of shear system, pressurization system, and data acquisition system from sitting to right. The set shear rate is 0.2 kPa/min, the deformation is controlled by 20 mm, and the data recording interval is 0.1 mm.

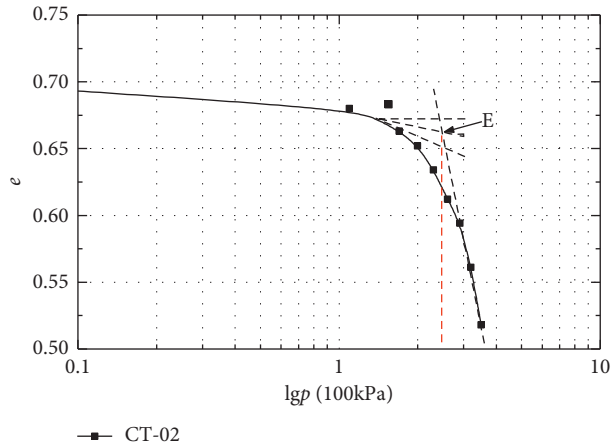

Figure 3: e-lgp curve of CT-02 of intact sample.

Table 9: Scheme of triaxial compression test.

Sample no.	Sample type	Test no.	Axial stress $\sigma 1$ (kPa)	Confining pressure $\sigma 3$ (kPa)	Consolidation ratio K_0	Note
D14-01	Undisturbed	TC-01	204	88	0.43	Consolidation ratio depends on the survey report
	Remolded	TC-02	204	88	0.43	
D14-02	Undisturbed	TC-03	273	114	0.42	
	Remolded	TC-04	273	114	0.42	

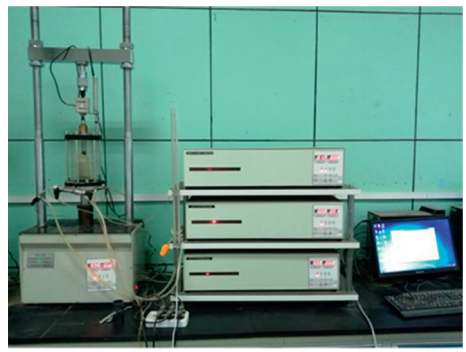

Figure 4: SLB-1A stress-strain controlled triaxial creep tester.

4.3. Test Results of D14-01 Triaxial Consolidated Undrained Shear Test

4.3.1. Stress-Strain Relationship. In our test, the lateral stress is controlled to decrease gradually, the axial stress is increased gradually, and the average principal stress is kept unchanged. Figures 5 and 6 are the stress-strain curves of the triaxial test of axial loading and lateral unloading of sample D14-01, undisturbed sample TC-01, and remolded sample TC-02 after K_0 consolidation (consolidation ratio is 0.43). As illustrated in Figures 6 and 7, the stress-strain curves of undisturbed sample TC-01 and remolded sample TC-02 are strain softening curves. When the strain exceeds 1.8%, the strain of undisturbed sample TC-01 begins to increase. When the strain exceeds 15%, the effective principal stress difference decreases from 241.7 kPa to 159.7 kPa (the strain is 20.3%), with an obvious steep drop process. When the strain exceeds 1.0%, the stress of remolded sample TC-02 begins to increase, the increase range is small, and remains at about 185kpa. When the strain exceeds 12%, the effective principal stress difference decreases to 177.7 kPa (the strain is 17.93%), and there is no obvious steep drop process. To sum up, the undisturbed sample shows an obvious structure.

4.3.2. Effective Stress Path. Figures 7 and 8 are the test effective stress path p'-q' curves of sample D14-01, undisturbed sample TC-01, and remolded sample TC-02, respectively. The change law of the effective stress path curve of the undisturbed sample TC-01 and the remolded sample TC-02 is the same, and the curve remains at the line with the average effective principal stress of 146 kPa. After the sample is damaged, the stress path deflects, and the average effective principal stress p' and the average effective principal stress difference q' decrease. While the sample is damaged, the average effective principal stress difference of undisturbed

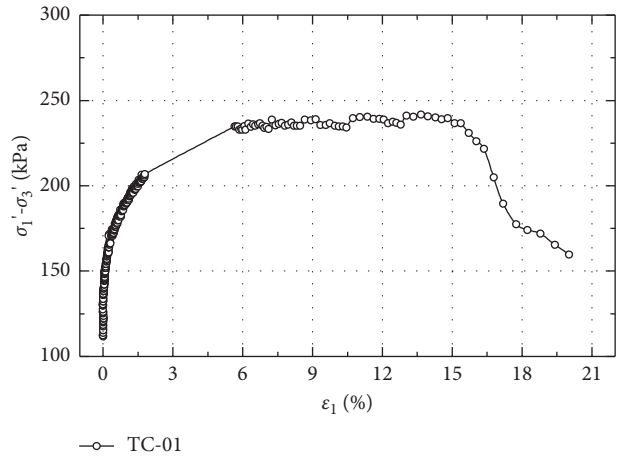

Figure 5: Stress strain relationship of undisturbed sample TC-01.

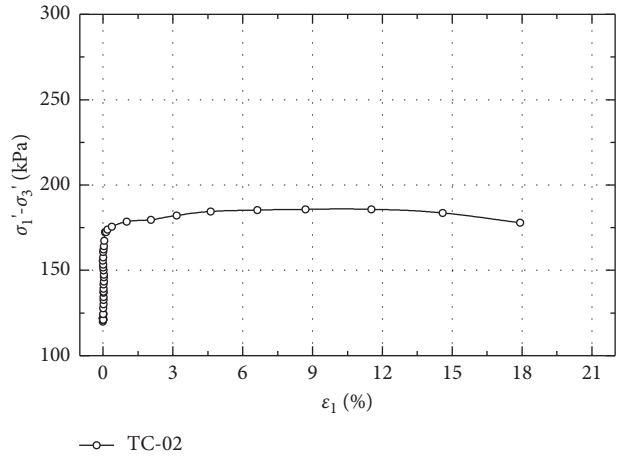

Figure 6: Stress strain relationship of TC-02 remolded sample.

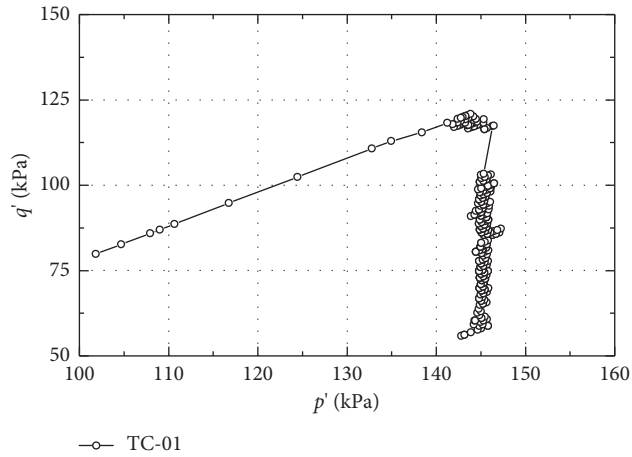

Figure 7: Test stress path of undisturbed sample TC-01.

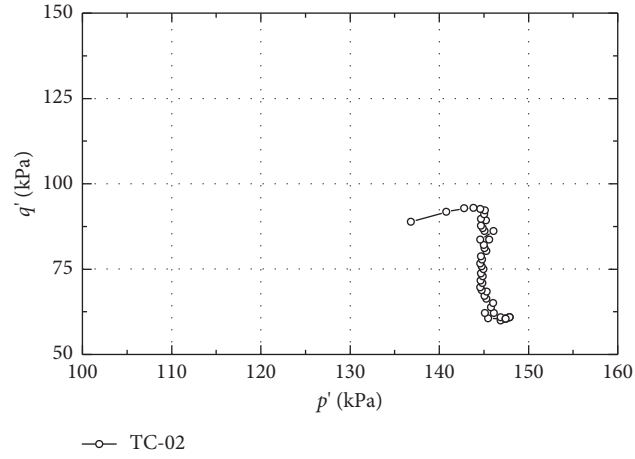

Figure 8: Stress path of remolded sample TC-01.

sample TC-01 is 120.85 kPa and that of remolded sample TC-02 is 92.6 kPa.

4.3.3. Consolidation Ratio K_0. Figures 9 and 10 show the change curves of consolidation ratio during the test shear of sample D14-01, undisturbed sample TC-01, and remolded sample TC-02, respectively. It can be seen from the figure that from the initial state, the consolidation ratio K_0 is 0.43, which gradually decreases with the strain and remains in a certain value range. The final consolidation ratio K_0 of undisturbed sample TC-01 is about 0.10 and that of remolded sample TC-02 is about 0.21.

4.4. Test Results of D14-02 Triaxial Consolidated Undrained Shear Test

4.4.1. Stress-Strain Relationship. Figures 11 and12 show the stress-strain relationship curves of axial loading and lateral unloading triaxial test of sample D14-02, undisturbed sample TC-03, and remolded sample TC-04 after K_0 consolidation (consolidation ratio is 0.42). It can be seen from the figure that the stress-strain curves of undisturbed sample TC-03 are strain softening curves, and the stress-strain curves of remolded sample TC-04 are weak strain hardening curves. When the strain exceeds 0.5%, the strain of the undisturbed sample TC-03 begins to increase, and the effective principal stress difference quickly reaches the peak value of 314.2 kPa. When the strain exceeds 4%, the effective principal stress difference begins to decrease to 266.3 kPa (the strain is 13.0%), with an obvious steep drop process, and then increases. When the strain exceeds 0.3%, the strain of remolded sample TC-04 begins to increase, and the corresponding stress increases little, which maintains at about 225.0 kPa, without obvious steep drop process. The undisturbed sample shows the structure clearly.

4.4.2. Effective Stress Path. Figures 13 and 14 are the test effective stress path p'-q' curves of sample D14-02, undisturbed sample TC-03, and remolded sample TC-04, respectively. As is shown in the figure, the change law of the effective stress path curve of the undisturbed sample TC-03 and the remolded sample TC-04 is basically the same, and the curve remains at the line with the average effective principal stress of 193.5 kPa. After the sample is damaged, the stress path deflects, and the average effective principal stress p' and the average effective principal stress difference q' decrease. When the sample is damaged, the average effective principal stress difference of undisturbed sample TC-03 is 158.2 kPa, and the average effective principal stress difference of remolded sample TC-04 is 113.4 kPa.

4.4.3. Consolidation Ratio K_0. Figures 15 and 16 are the change curves of consolidation ratio during test shear of sample D14-02, undisturbed sample TC-03, and remolded sample TC-04, respectively. As the graphs show, the consolidation ratio K_0 is 0.42 in the initial state, which gradually decreases with the strain and remains in a certain value range. The final consolidation ratio K_0 of undisturbed sample TC-03 is about 0.10 and that of remolded sample TC-04 is about 0.25.

5. Triaxial Compression Drainage Test

5.1. Pilot Protocol. Due to experimental requirements, the effective cohesion c' and effective internal friction angle of undisturbed and remolded samples are determined according to the test requirements ϕ'. Therefore, we need to make four test schemes, and the effective confining pressure of each group is 100, 200, and 300 kPa. The test scheme is presented comprehensively in Table 10.

5.2. Test Methods. the consolidated drained shear test (CD test) has two stages, and one is consolidation stage and the other is shear stage. In the consolidation stage, constant surrounding pressure is applied to the soil sample to measure the displacement and the dissipation process of pore water pressure. After consolidation, the soil sample is sheared at a constant strain rate under the condition of drainage, and the shear failure resistance of the soil sample is measured.

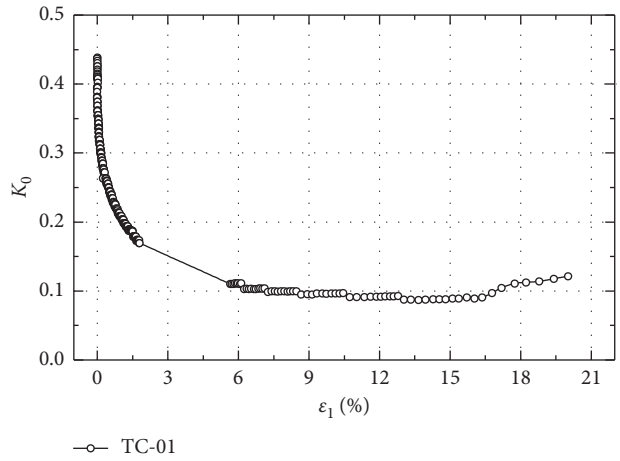

Figure 9: Variation curve of TC-01 consolidation ratio K_0 of undisturbed sample.

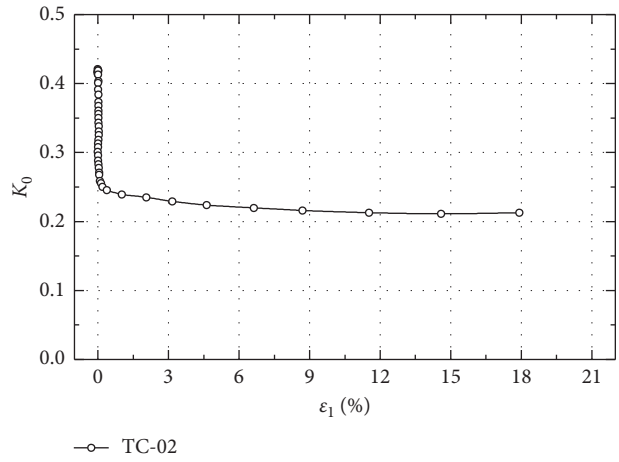

Figure 10: Variation curve of TC-02 consolidation ratio K_0 of remolded sample.

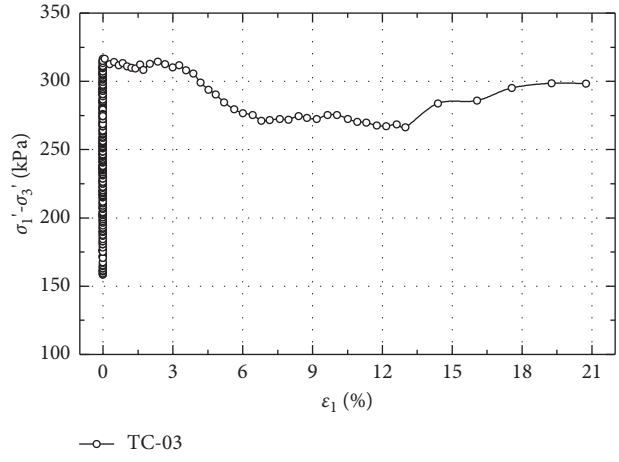

Figure 11: Stress strain relationship of undisturbed sample TC-01.

Sample installation: at first, take out the cylindrical sample to be tested ($\Phi 39.1 \times 80$ mm) and wrap the rubber membrane on the outside of the sample with a membrane bearing cylinder and a suction ball. Secondly, clamp the filter paper and water permeable stone up and down, tie the lower end of the rubber membrane with the base and the upper end with the upper cover with a rubber ring, and install the pressure chamber cover. Then, open the water filling switch, fill the pressure chamber with water, close the upper exhaust valve, seal the pressure chamber, and prepare for the test;

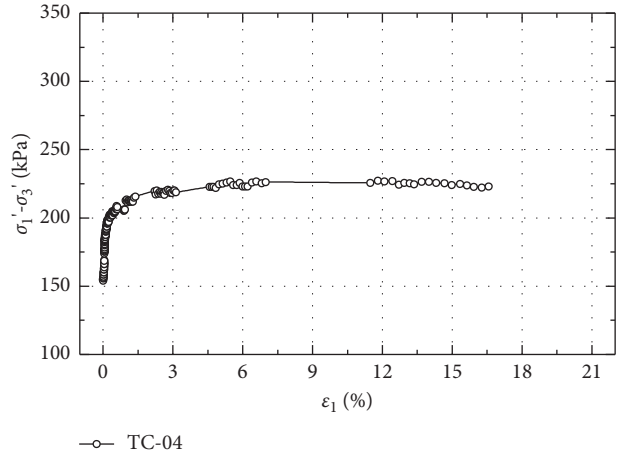

Figure 12: Stress strain relationship of TC-02 remolded sample.

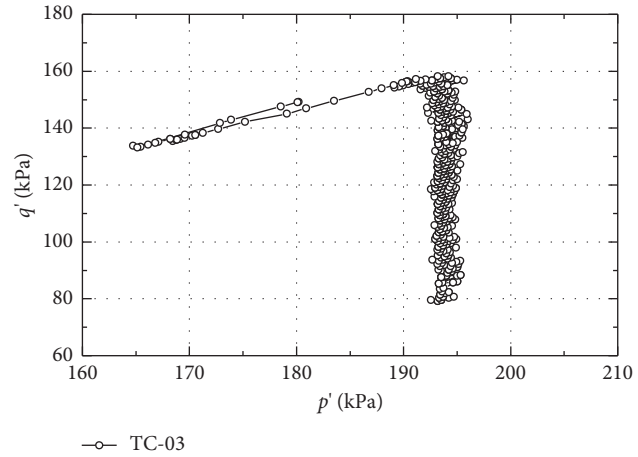

Figure 13: Stress path of undisturbed sample TC-03.

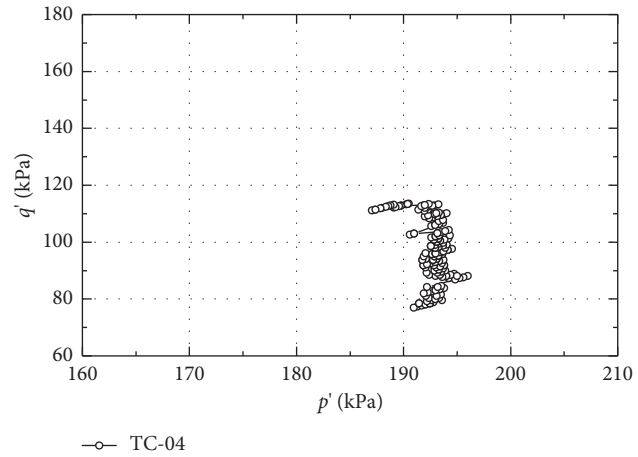

Figure 14: Stress path of remolded sample TC-04.

Consolidation stage: first, open the operation interface of the test system. Next, set the project number and corresponding ambient pressure (100/200/300 kPa), and sample once in 240 s, which measures both displacement and pore water pressure. And the test termination condition ends when consolidation time is 24 h; shear stage: firstly, open the operation interface of the test system and set both the project number and the corresponding ambient pressure (100/200/300 kPa). And then, set the strain rate to 0.1 mm/min. Finally, measure the parameters including principal stress

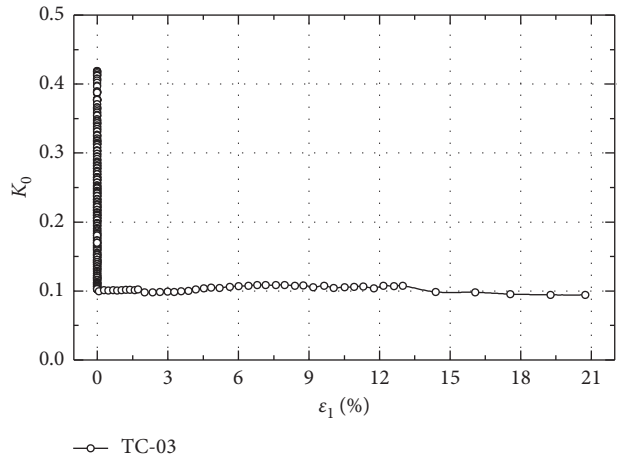

Figure 15: Variation curve of TC-03 consolidation ratio K_0 of undisturbed sample.

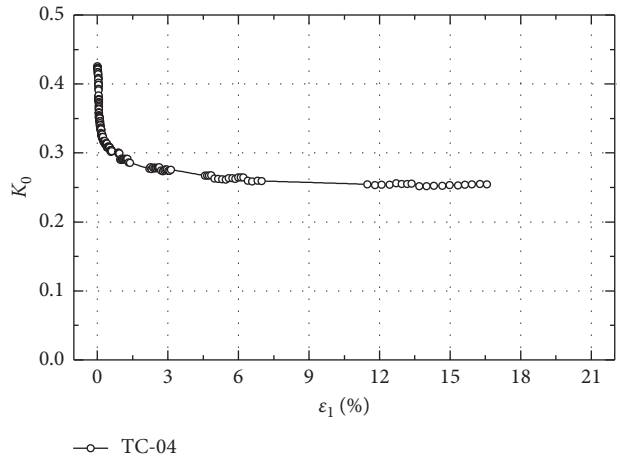

Figure 16: Variation curve of TC-04 consolidation ratio K_0 of remolded sample.

difference, axial deformation, pore water pressure, and axial deformation, and record the data every 0.1 mm, and test termination condition happens when axial deformation is greater than 20 mm.

5.3. Specimen D14-01 Triaxial Consolidated Drainage Shear Test Results

5.3.1. Stress-Strain Relationship. Figures 17 and 18 are the stress-strain curves of triaxial consolidated drained shear test of sample D14-01, undisturbed sample, and remolded sample, respectively. As can be seen from the Figures 18 and 19, the stress-strain relationship curve of undisturbed sample is a strain softening curve, and the stress-strain relationship curve of remolded sample is a weak strain hardening curve.

5.3.2. Shear Strength Parameters. Figures 19 and 20 are K_f' line and ϕ' line of undisturbed sample and remolded sample of sample D14-01. We can calculate the effective stress intensity index according to the K_f' line and ϕ' line. The effective cohesion of the undisturbed sample of sample D14-01 is 71.1 kPa and the effective internal friction angle is 25.3°. The effective cohesion of the remolded sample of sample D14-01 is 28.7 kPa and the effective internal friction angle is 26.8°.

5.4. Specimen D14-02 Triaxial Consolidated Drainage Shear Test Results

5.4.1. Stress-Strain Relationship. Figures 21 and 22 are the stress-strain curves of triaxial consolidated drained shear test of sample D14-02, undisturbed sample, and remolded sample, respectively. As it can be seen, the stress-strain relationship curve of undisturbed sample is a strain softening curve, and the stress-strain relationship curve of remolded sample is a weak strain hardening curve.

5.4.2. Shear Strength Parameters. Figures 23 and 24 show K_f' line and ϕ' line of undisturbed sample and remolded sample of sample D14-02. As shown in the figure, we can calculate

Table 10: Consolidated drained triaxial test scheme.

Sample no.	Sample type	Test no.	Effective containment pressure (kPa)
D14-01	Undisturbed	CD01-100	100
		CD01-200	200
		CD01-300	300
	Remolded	CD02-100	100
		CD02-200	200
		CD02-300	300
D14-02	Undisturbed	CD03-100	100
		CD03-200	200
		CD03-300	300
	Remolded	CD04-100	100
		CD04-200	200
		CD04-300	300

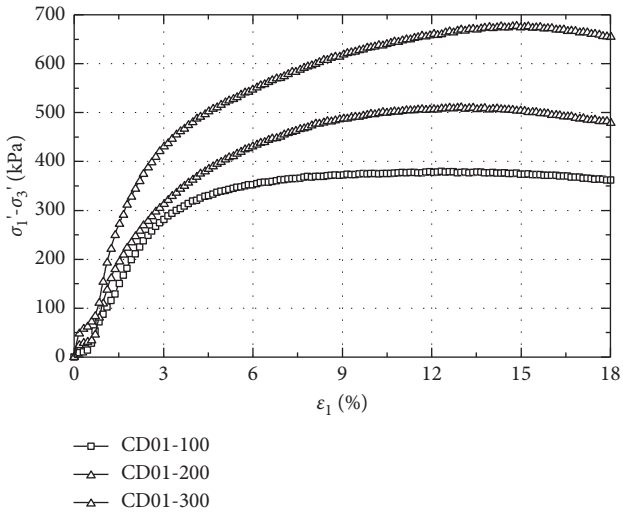

Figure 17: Stress strain relationship of TC-01 undisturbed sample.

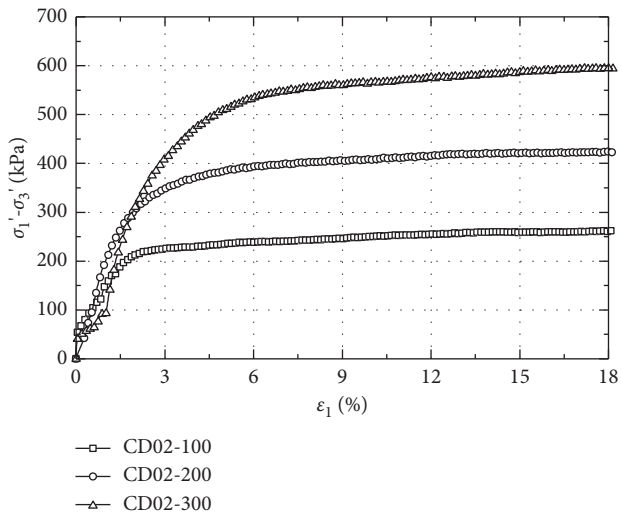

Figure 18: Stress strain relationship of TC-02 remolded sample.

the effective stress intensity index according to the K_f' line and ϕ' line. The effective cohesion of the undisturbed sample D14-02 is 80.4 kPa and the effective internal friction angle is 30.9°. The effective cohesion of the remolded sample of sample D14-02 is 14.3 kPa and the effective internal friction angle is 30.7° (Figure 24).

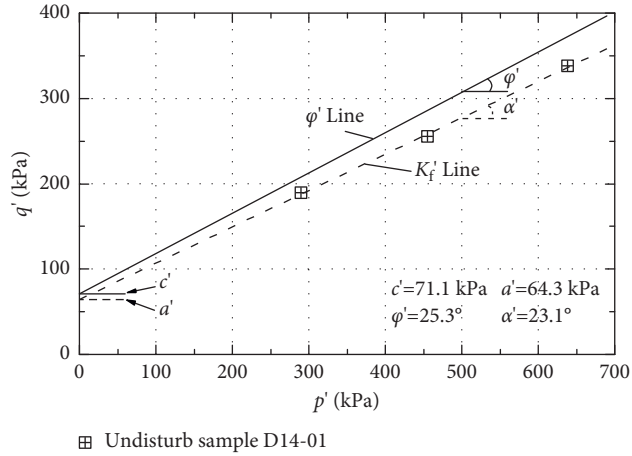

Figure 19: $(K)_f$ line and ϕ' line of undisturbed sample D14-01.

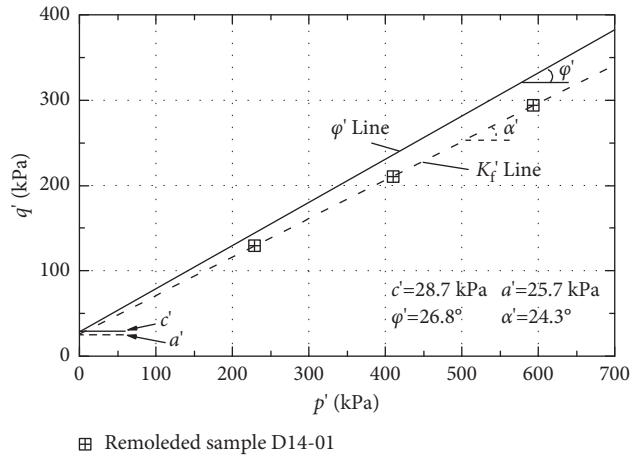

Figure 20: $(K)_f$ line and ϕ' line of remolded sample D14-01.

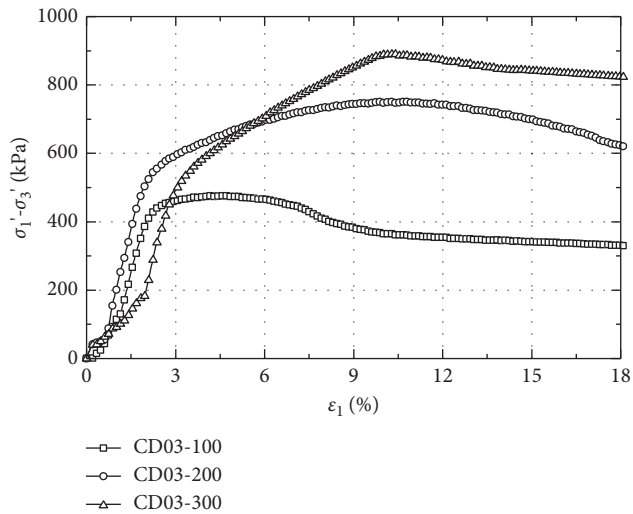

Figure 21: Stress strain relationship of D14-02 undisturbed sample.

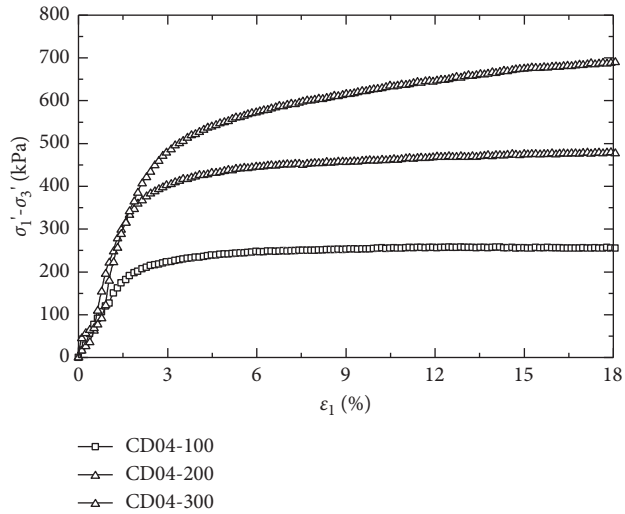

Figure 22: Stress strain relationship of D14-02 remolded sample.

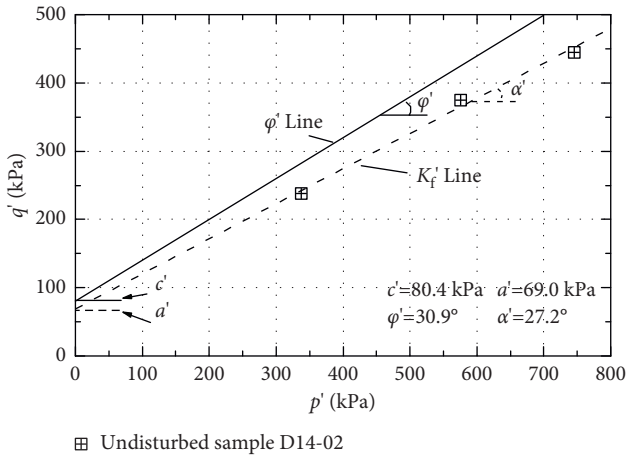

Figure 23: $(K)_f$ line and ϕ' line of undisturbed sample D14-02.

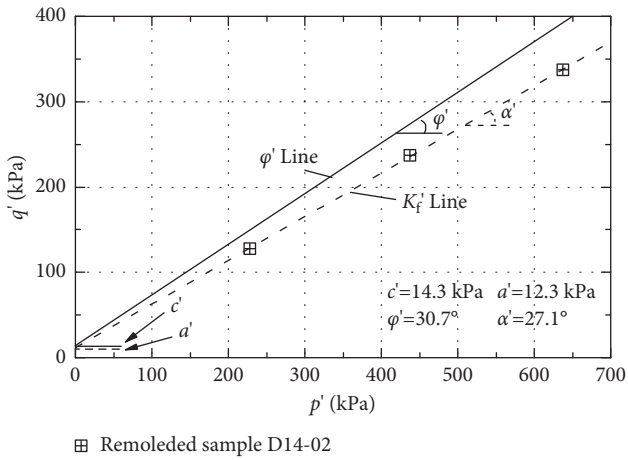

Figure 24: $(K)_f$ line and ϕ' line of remolded sample D14-02.

6. Conclusion

Firstly, the structure has an obvious influence on the stress-strain relationship of the sample. In the triaxial undrained and drained experiments, the stress-strain relationship curve of the undisturbed sample is a strain softening curve and the stress-strain relationship curve of the remolded sample is a weak strain hardening curve. Secondly, in the same loading conditions, the shear strength of undisturbed soil is significantly higher than that of remolded soil in triaxial undrained and drained experiments. Finally, in the triaxial test of undisturbed and remolded samples, the change law of consolidation ratio is basically the same. The consolidation ratio decreases gradually with the axial strain and finally stabilizes at a fixed value. But the final consolidation ratio of remolded soil is greater than that of undisturbed soil.

Data Availability

The data supporting the conclusion of the article are shown in the relevant figures and tables in the article.

Conflicts of Interest

The authors declare that there are no conflicts of interest regarding the publication of this article.

Acknowledgments

This work was financially supported by the Henan Natural Science Foundation 212300410327 and the Scientific and Technological Project in Henan Province 222102320173.

References

[1] S. T. Zhao, Y. T. Xu, Z. W. Cheng, J. F. Ren, and D. Jiang, "Circuit breaker mechanical characteristic parameters measurement based on machine vision," *Applied Mechanics and Materials*, vol. 687-691, pp. 934–937, 2014.

[2] A. Pkla, A. Mesbah, V. Rigassi, and J. C. Morel, "Comparaison de méthodes d'essais de mesures des caractéristiques mécaniques des mortiers de terre," *Materials and Structures*, vol. 36, no. 2, pp. 108–117, 2003.

[3] N. S. Dharmesh Lal and S. Chandrakaran, "Triaxial test on saturated sands reinforced with coir products," *International Journal of Geotechnical Engineering*, vol. 13, no. 3-4, pp. 270–276, 2019.

[4] Y. Q. Hu and W. K. Binienda, "Multiscale Modeling of a Notched Coupon Test for Triaxially Braided Composites," *Key Engineering Materials*, vol. 795, 2019.

[5] S. Zhang, G. Ye, and J. Wang, "Elastoplastic model for overconsolidated clays with focus on volume change under general loading conditions," *International Journal of Geomechanics*, vol. 18, no. 3, Article ID 04018005, 2018.

[6] N. Li, H. Wang, B. Ma, and R. Li, "Investigation of unbound granular material behavior using precision unbound material analyzer and repeated load triaxial test," *Transportation Geotechnics*, vol. 18, pp. 1–9, 2019.

[7] D. Jadhav, H. Jambhulkar, S. Jaybhaye et al., "An Experimental Study of Clayey Soil with Rice Husk Ash Using Triaxial Test," *Iosr Journal of Mechanical & Civil Engineering*, vol. 15, no. 3, pp. 45–50, 2018.

[8] J. K. Mitchell, K. Soga, and J. K. Mitchell, *Fundamentals of Soil Behavior*, Wiley, New Jersey, NY, USA, 1976.

[9] J. B. Burland, "On the compressibility and shear strength of natural clays," *Géotechnique*, vol. 40, no. 3, pp. 329–378, 1990.

[10] C. Ovalle and G. Arenaldi-Perisic, "Mechanical behaviour of undisturbed diatomaceous soil," *Marine Georesources & Geotechnology*, vol. 39, no. 6, pp. 1–8, 2020.

[11] R. G. U. Sousa, I. B. de Oliveira, S. L. Machado, and M. de Fátima Carvalho, "Solute dispersion of organic compounds on undisturbed soil columns," *Transport in Porous Media*, vol. 132, no. 2, pp. 267–282, 2020.

[12] K. S. Freitas, R. A. Armindo, L. F. Pires, V. S. Filho, and S. R. Júnior, "A method to determine the soil bulk density of undisturbed samples with non-isodiametric shape," *Soil and Tillage Research*, vol. 191, pp. 344–352, 2019.

[13] Y. Xu, P. Guo, C. Zhu, G. Lei, and K. Cheng, "Experimental investigation into compressive behaviour and preconsolidation pressure of structured loess at different moisture contents," *Geofluids*, vol. 2021, no. 3, pp. 1–9, Article ID 5585392, 2021.

[14] S. M. Haeri, A. Zamani, and A. A. Garakani, "Collapse potential and permeability of undisturbed and remolded loessial soil samples," *Unsaturated Soils: Research and Applications*, vol. 2021, no. 4, pp. 301–308, 2012.

[15] B. Gao and L. Su, "Triaxial mechanical testing of undisturbed unsaturated loess," *Soil Mechanics and Foundation Engineering*, vol. 57, no. 1, pp. 57–64, 2020.

[16] F. Y. Chu, "Study on engineering characteristics of coarse-grained soil based on large-scale triaxial test," *Advanced Materials Research*, vol. 936, pp. 1387–1392, 2014.

[17] D. W. Airey, "Triaxial testing of naturally cemented carbonate soil," *Journal of Geotechnical Engineering*, vol. 119, no. 9, pp. 1379–1398, 1993.

[18] Z. H. Chen, X. W. Fang, Y. Q. Zhu, B. Qin, X. W. Wei, and Z. H. Yao, "Research on meso-structures and their evolution laws of expansive soil and loess," *Yantu Lixue/Rock and Soil Mechanics*, vol. 30, no. 1, pp. 1–11, 2009.

[19] S. Nokande, M. A. Khodabandeh, S. S. Hosseini, and S. M. Hosseini, "Collapse potential of oil-contaminated loessial soil (case study: golestan, Iran)," *Geotechnical & Geological Engineering*, vol. 38, no. 1, pp. 255–264, 2020.

[20] H. Wang, H. Sun, Z. Huang, and X. Ge, "A microstructural investigation on hydraulic conductivity of soft clay," *Bulletin of Engineering Geology and the Environment*, vol. 80, no. 4, pp. 4067–4078, 2021.

[21] N. Jiang, C. Wang, Q. Wu, and S. Li, "Influence of structure and liquid limit on the secondary compressibility of soft soils," *Journal of Marine Science and Engineering*, vol. 8, no. 9, 627 pages, 2020.